AAS 19-287

ATTITUDE MANEUVER DESIGN FOR PLANAR SPACE SOLAR POWER SATELLITES

Michael A. Marshall,* Ashish Goel,† and Sergio Pellegrino‡

This paper investigates the attitude dynamics of a planar space solar power satellite (SSPS) by formulating the power-optimal guidance problem as a nonlinear trajectory optimization problem. The power-optimal guidance problem determines the orientation of an SSPS throughout its orbit that maximizes the amount of power transmitted to Earth. This transmitted power is a function of the relative geometry between the SSPS, the Sun, and the receiving station. Hence, it is inherently coupled to the attitude of the SSPS, i.e., the orientation that maximizes power transmission changes as the relative geometry changes. We first approximate the discretized trajectory optimization problem as a quadratic program (QP). We then solve the QP to obtain attitude trajectory designs for various orbits. These solutions highlight how maximizing transmitted power typically requires large slew maneuvers. Ultimately, by quantifying control and propellant requirements for various orbits, we emphasize how maneuver dynamics play an important role in SSPS design.

INTRODUCTION

Space solar power is the concept of collecting solar power in space and wirelessly transmitting it to Earth. Compared to terrestrial solar power, space solar has several benefits. For one, it decouples solar power collection from terrestrial weather and diurnal and seasonal cycles, meaning a space solar power system can potentially provide clean, renewable base load power to the electrical grid without the need for expensive energy storage solutions (e.g. batteries). Additionally, space solar has the capability to beam power to virtually any location on Earth at any time, irrespective of latitude or weather condition, making it an attractive technology for powering resource-deprived regions.

While the science fiction author Isaac Asimov presented the original idea for space solar in 1941,[1] another two decades passed before P. E. Glaser proposed the first realistic concept for a space solar power satellite (SSPS).[2] In the years since, researchers have proposed a variety of SSPS concepts,[3–6] all of which are effectively variations of the original concept proposed by Glaser. These "classical" concepts feature large, monolithic spacecraft with large photovoltaic (PV) arrays that convert solar power to direct current (DC) power, DC to radio frequency (RF) converters, and one or more antennas for beaming RF energy to Earth. They also typically include either *mechanically steerable* solar arrays or antennas that decouple the problems of antenna steering and sun pointing.

However, reducing mass is imperative for realizing an economically viable space solar power system.[7] In other words, economic viability requires ultralight structures. Innovative new structural concepts characterized by extremely low areal mass densities (on the order of 1 kg/m^2 or less) are driving the development of ultralight, planar SSPS concepts.[8] These concepts replace large, monolithic spacecraft with clusters of

*Graduate Research Assistant, Graduate Aerospace Laboratories, 1200 E. California Blvd., Mail Code 105-50, Pasadena, CA 91125. mmarshall@caltech.edu

†Postdoctoral Researcher, Jet Propulsion Laboratory, 4800 Oak Grove Dr., Pasadena, CA 91109. ashish.goel@jpl.nasa.gov

‡Joyce and Kent Kresa Professor of Aerospace and Civil Engineering; Jet Propulsion Laboratory Senior Research Scientist; Co-Director, Space-Based Solar Power Project, Graduate Aerospace Laboratories, 1200 E. California Blvd., Mail Code 105-50, Pasadena, CA 91125. sergiop@caltech.edu

smaller spacecraft and replace complicated mechanical systems with lightweight, planar elements that integrate PV surfaces, DC-to-RF converters, and microwave patch antennas, like those described in Jaffe and McSpadden (2013)[9] and Gdoutos et al. (2018).[10]

Planarity is a design decision that simplifies the structural architecture and facilitates efficient packaging of the SSPS.[8] As a consequence of planarity, the problems of orienting the PV surface towards the Sun and directing the RF beam towards a receiving station on Earth are intrinsically coupled, i.e., reorienting the PV surface reorients the RF surface and vice versa. This is a critical difference between classical and planar SSPS architectures. Due to this PV-RF surface coupling, maximizing power transfer requires demanding slew maneuvers.[11] The combination of attitude agility and structural flexibility leads to coupling between the spacecraft's attitude and structural dynamics. Not surprisingly, attitude maneuver dynamics are key structural design drivers for a planar SSPS. Thus, quantifying attitude maneuver dynamics is important for future studies of modal excitation and inertial loading on the structure. Additionally, important system level considerations, including attitude control system (ACS) sizing and ACS propellant consumption, are linked to attitude maneuver dynamics.

The baseline SSPS design considered in this paper consists of two primary layers. The top layer is composed of PV cells that convert solar radiation to DC electrical power. The DC electrical power is then fed into integrated circuits (ICs) that convert DC electrical power to RF power. The bottom layer consists of tiny patch antennas that radiate RF power towards Earth. The patch antennas are synchronized to operate as a steerable phased array. Throughout this paper, this baseline module design is referred to as single-sided PV, single-sided RF (PV1RF1).

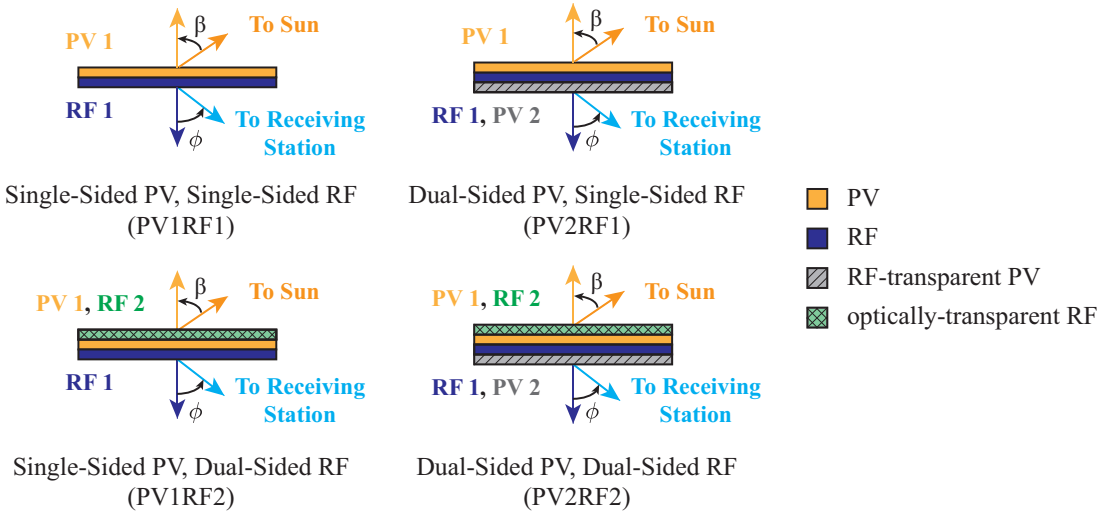

Figure 1: **Baseline SSPS Design and Dual-Sided Variations**

Several "dual-sided" variations of this baseline design have also been proposed. Dual-sided refers to an SSPS with at least two PV surfaces or two RF surfaces. A dual-sided SSPS is constructed by adding either a layer of PV-transparent antennas or RF-transparent PV cells to the top or bottom layers of the baseline design. Throughout this paper, we refer to a module with two PV surfaces and one RF surface as dual-sided PV, single-sided RF (PV2RF1). Similarly, modules with one PV surface and two RF surfaces or two PV surfaces and two RF surfaces are referred to as single-sided PV, dual-sided RF (PV1RF2) or dual-sided PV, dual-sided RF (PV2RF2), respectively. Note that for any dual-sided SSPS, only a single PV surface and a single RF surface operate at any given time. These four SSPS designs are depicted in Figure 1 where β and ϕ denote the sun and squint angles, i.e., the orientations of the top PV surface relative to the Sun and the bottom RF surface relative to the receiving station. Dual-sided operations can increase transmitted power by upwards of 50%. However, maximizing power transmission during dual-sided operations requires large slew maneuvers.[11] Due to practical considerations, we focus on the PV2RF1 architecture in this paper, but we also

briefly study the PV1RF1 architecture for comparison.

Various authors have studied attitude dynamics and control of classical SSPS concepts.[6,12–15] However, aside from two notable exceptions, attitude dynamics and control for planar SSPS concepts are largely unexplored in the literature. In particular, Goel et al. (2017)[16] presents a preliminary study of the attitude dynamics of both PV1RF1 and PV1RF2 SSPSs in geostationary Earth orbit (GEO). Likewise, Goel et al. (2017)[17] investigates the attitude dynamics of a PV1RF2 SSPS in the context of formation flying in GEO. To that end, this paper complements the existing literature by investigating the attitude dynamics of an SSPS in both GEO and a representative medium Earth orbit (MEO). To our knowledge, this is the first investigation of the attitude dynamics of a PV2RF1 SSPS and of any planar SSPS in MEO. Moreover, whereas Goel et al. (2017)[16] and Goel et al. (2017)[17] consider the concentrated PV system from Gdoutos et al. (2018),[10] this work investigates the attitude dynamics of an SSPS with a planar, non-concentrated PV system. Additionally, a key goal of the current work is to provide tools for quantifying the inertial loads on the spacecraft due to attitude maneuvers. These loads are critical for future studies of flexible spacecraft.

This paper is divided into four sections. In the first section, we summarize the power-optimal guidance problem for a planar SSPS from Marshall et al. (2018).[11] The second section starts from the power-optimal guidance problem to formulate the problem of attitude maneuvering for optimum power transfer as a trajectory optimization problem. The third section presents the results of case studies for a 25 m $\times$ 25 m SSPS concept in both GEO and a 20,184 km MEO. The final section then discusses future research directions and the ramifications of this work on SSPS design.

REVIEW OF POWER-OPTIMAL GUIDANCE PROBLEM

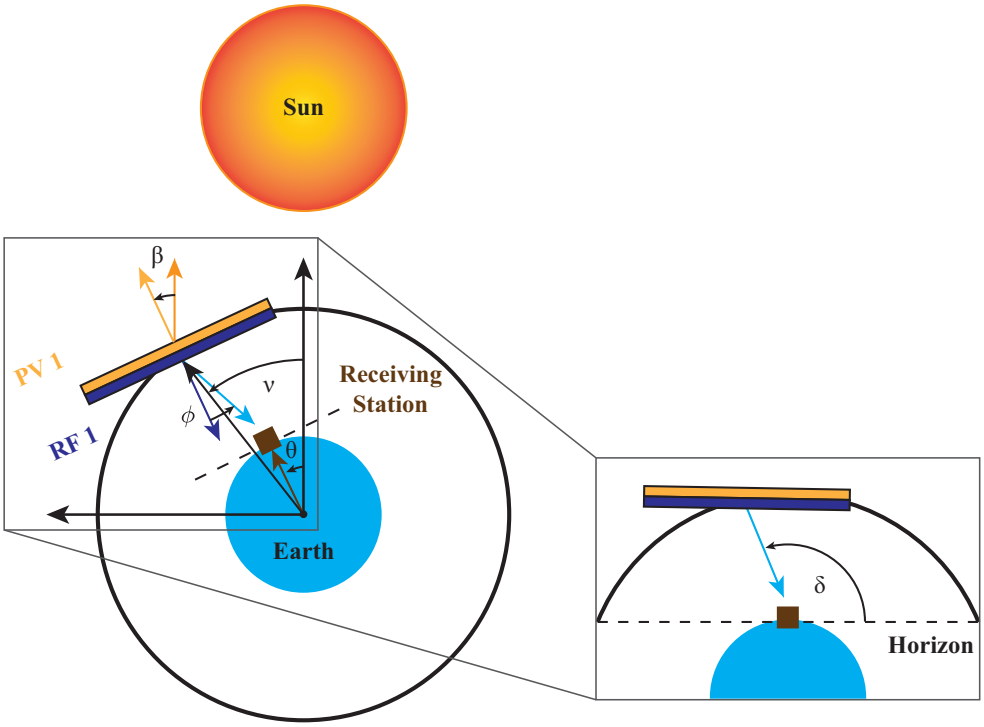

Figure 2: **SSPS-Sun-receiving station geometry. While the figure depicts a single-sided PV, single-sided RF SSPS, it is equally applicable for any SSPS design.**

In this section, we summarize the power-optimal guidance problem from Marshall et al. (2018)[11] for a planar SSPS in a circular, equatorial orbit transmitting to an equatorial receiving station. We leverage the power-optimal guidance framework to formulate the attitude maneuver design problem.

The power-optimal guidance problem defines the orientation of an SSPS that maximizes power transfer to the receiving station. Maximizing power transfer maximizes the cumulative energy delivered to the electrical grid. The total transmitted power strongly depends on the geometry of the SSPS relative to the Sun and Earth receiving station and is characterized by the sun angle (β), squint angle (ϕ), Earth Rotation Angle, or ERA (θ), and satellite elevation angle (δ), as depicted in Figure 2. The sun and squint angles define the orientations of the SSPS with respect to the Sun and receiving station, respectively. The ERA describes the position of the receiving station on Earth's surface in inertial space and the elevation angle describes the position of the SSPS relative to the receiving station. These four angles are geometrically related by

$$\beta + \phi = \delta + \theta - \frac{\pi}{2} \tag{1}$$

where $\delta = \delta(\nu)$ and

$$\theta = \omega_{\oplus}\left(t - t_0\right) + \theta_0 \tag{2}$$

$\omega_{\oplus}$ is the rotation rate of Earth about its spin axis. Eq. (1) couples the attitude and orbit dynamics of the SSPS. Finally, for a circular orbit with mean motion n,

$$\nu = n\left(t - t_0\right) + \nu_0 \tag{3}$$

We assume that $\theta_0 = \nu_0 = 0$, i.e., that both the SSPS and receiving station start at local noon at time $t = 0$. Note that in GEO, $n = \omega_{\oplus}$ and $\delta = 90^{\circ}$, from which it follows that $\nu = \theta$ and $\beta + \phi = \theta$.

In this work, we adopt the assumptions discussed in Section II of Marshall et al (2018),[11] i.e., we assume that Earth's motion about the Sun is negligible for short time scales (e.g. a sidereal day), incident sunlight is collimated, the SSPS only rotates about the normal to the orbit plane, etc. Likewise, we neglect the Earth's tilt about its spin axis and orbit perturbations like solar radiation pressure. Under these assumptions, $\beta(t)$ fully describes the orientation of the SSPS.

Transmitted Power

The total power density per unit aperture area transmitted by the SSPS is

$$W_t(\beta, \phi) = W_{\mathrm{SF}}\eta_{\mathrm{PV}}\eta_{\text{DC-RF}}\,\mathrm{PV}(\beta)\,\mathrm{RF}(\phi)\,\mathrm{AF}(\phi) \tag{4}$$

where $W_{\mathrm{SF}} = 1361$ W/m^2 is the incident solar flux, η_{PV} is the optical-to-electrical power conversion efficiency of the PV cells, $\eta_{\text{DC-RF}}$ is the DC-to-RF conversion efficiency of the system, $\mathrm{PV}(\beta)$ is the efficiency of the PV cells as a function of sun angle, $\mathrm{RF}(\phi)$ is the efficiency of a single antenna in the phased array as a function of squint angle, and $\mathrm{AF}(\phi)$ is the phased array factor. Eq. (4) neglects the losses due to any impedance mismatch between the RF source and antenna. $W_t = 0$ in eclipse and when the Earth blocks the SSPS's view of the receiving station. It follows from Eq. (4) that the orientation that maximizes power collection is not necessarily the same as the orientation that maximizes power transfer.

We assume planar (non-concentrated) PV surfaces with a PV efficiency function that follows a cosine law with a minimum acceptance angle of 5°, i.e., for local sun angles that exceed the minimum acceptance angle, the PV efficiency function is $\mathrm{PV}(\beta) = |\cos(\beta)|$.

Likewise, we assume the RF layer consists of near-isotropic patch antennas with the RF efficiency function depicted in Figure 3. This RF efficiency function results from electromagnetic simulations of the patch antennas described in Gdoutos et al.[10] Finally, we approximate the array factor by a cosine loss, i.e. $\mathrm{AF}(\phi) = |\cos(\phi)|$. $\mathrm{PV}(\beta)$, $\mathrm{RF}(\phi)$, and $\mathrm{AF}(\phi)$ are all symmetric, periodic, positive semidefinite functions with fundamental periods of 180°, meaning W_t is also periodic with the same fundamental period.

Within the scope of this paper, W_{SF}, η_{PV}, and η_{DC-RF} are constants. As a result, we can define a normalized transmitted power density that only depends on the geometry in Figure 2, as follows:

$$\eta(\beta, \phi) = \frac{W_t(\beta, \phi)}{W_{\mathrm{SF}}\eta_{\mathrm{PV}}\eta_{\text{DC-RF}}} = \mathrm{PV}(\beta)\,\mathrm{RF}(\phi)\,\mathrm{AF}(\phi) \tag{5}$$

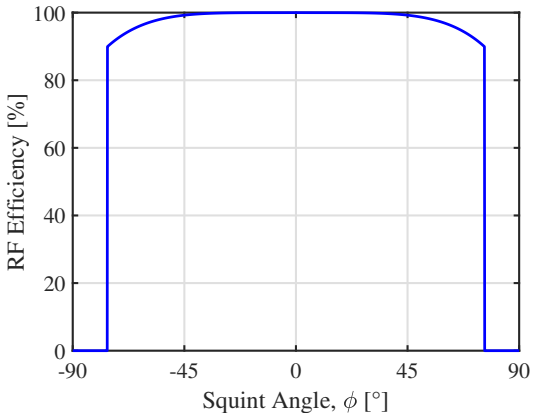

Figure 3: **RF Efficiency Function for a Near-Isotropic Patch Antenna**

η is hereafter referred to as the geometric efficiency. Maximizing η maximizes W_t and vice versa. Finally, substituting Eq. (1) into Eq. (5) allows the geometric efficiency to be rewritten as

$$\eta(\beta) = \mathrm{PV}(\beta)\,\mathrm{RF}\left(\delta + \theta - \beta - \frac{\pi}{2}\right)\mathrm{AF}\left(\delta + \theta - \beta - \frac{\pi}{2}\right) \tag{6}$$

where δ and θ are known from the orbit. As a result, η is effectively a single-variable function of β. For any (δ, θ), we can use Eq. (6) to determine the orientation that maximizes transmitted power.

Pointing Constraints

Let $\mathbf{n}_{\mathrm{PV}}$ denote the outward normal vector from a planar PV surface. If $\mathbf{s}$ denotes the sun vector, then the surface collects power so long as

$$\mathbf{n}_{\mathrm{PV}} \cdot \mathbf{s} = \cos(\beta) > 0 \tag{7}$$

Similarly, for a planar RF surface with outward normal vector $\mathbf{n}_{\mathrm{RF}}$ radiating towards a receiving station in direction $\mathbf{r}$, the surface transmits power so long as

$$\mathbf{n}_{\mathrm{RF}} \cdot \mathbf{r} = \cos(\phi) > 0 \tag{8}$$

Eqs. (7) and (8) result in the following pointing constraints for single-sided PV and single-sided RF surfaces:

$$-90^\circ < \beta < 90^\circ \tag{9}$$

$$-90^\circ < \phi < 90^\circ \tag{10}$$

where ϕ is related to β through Eq. (1). Because attitude is modulo 360°, i.e., a rotation of β by an integer multiple of 360° physically results in the same attitude, and $W_t = 0$ if either β or ϕ are integer multiples of 90°, there are no pointing constraints for a dual-sided surface.

Table 1: **SSPS Pointing Constraints**

Design	Sun Angle	Squint Angle
Single-Sided PV, Single-Sided RF	$-90^\circ < \beta < 90^\circ$	$-90^\circ < \phi < 90^\circ$
Dual-Sided PV, Single-Sided RF	$-\infty < \beta < \infty$	$-90^\circ < \phi < 90^\circ$
Single-Sided PV, Dual-Sided RF	$-90^\circ < \beta < 90^\circ$	$-\infty < \phi < \infty$
Dual-Sided PV, Dual-Sided RF	$-\infty < \beta < \infty$	$-\infty < \phi < \infty$

Table 1 summarizes the resulting pointing constraints for the four SSPS designs from Figure 1.* In all cases, we enforce squint angle limits by mapping squint angles to sun angles using Eq. (1). Note that $W_t = 0$ if it is impossible to satisfy the pointing constraints for some particular orbit geometry.

Power-Optimal Guidance Problem

The power-optimal guidance problem maximizes power (and energy) transmission to the receiving station subject to appropriate pointing constraints. We can formulate the power-optimal guidance problem as follows:

Problem 1:

$$\max_{\beta(t)} \int_0^{t_f} \eta(\beta(t))\, \mathrm{d}t \qquad \text{subject to:} \qquad \begin{cases} |\beta(t)| < \beta_{\max} \\ |\phi(t)| < \phi_{\max} \end{cases}$$

where t_f is the final simulation time, typically taken to be either the orbit period or the length of a sidereal day, and $\beta_{\max}$ and $\phi_{\max}$ are pointing constraints from Table 1. We denote solutions to the power-optimal guidance problem by $\beta^*(t)$. $\beta^*(t)$ is a purely kinematic solution that maximizes transmitted power independent of a spacecraft's dynamics. The corresponding geometric efficiency is $\eta^*(t)$. Marshall et al. (2018)[11] details several known solutions for geostationary, medium, and low Earth orbits. These solutions provide reference trajectories for the attitude maneuver design problem.

ATTITUDE MANEUVERING FOR OPTIMUM POWER TRANSFER

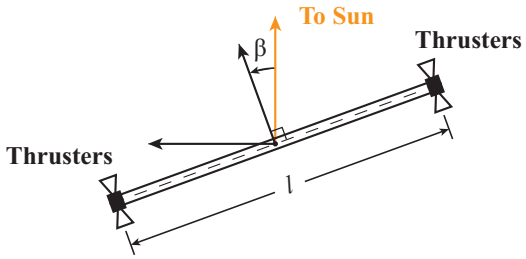

Figure 4: **Idealized, Rigid SSPS with Tip-Mounted Attitude Control Thrusters**

To study the problem of attitude maneuvering for optimum power transfer, we extend the power-optimal guidance problem (*Problem 1*) to account for attitude dynamics and control constraints. Within this paper, we consider an idealized, rigid SSPS with tip-mounted electrically-powered thrusters for attitude control, as depicted in Figure 4. The thrusters are bidirectional; two thrusters are fired simultaneously in opposite directions to form a couple. We intentionally neglect disturbances like gravity gradient torques because we are interested in guidance and dynamics, not attitude control. Hence, the attitude dynamics for our single degree-of-freedom SSPS are described by $\ddot{\beta}(t) = u(t)$ where $u(t)$ is the angular acceleration imparted by the thrusters and we have assumed that any mass property changes due to ACS propellant consumption are negligible. Note that this formulation of the dynamics is independent of the spacecraft's length scale and mass properties. Additionally, we enforce periodicity constraints on attitude and angular velocity so that system performance does not change from day to day.

Ultimately, we choose an objective function that maximizes power transmission and minimizes propellant consumption. The resulting optimization problem is

Problem 2:

$$\min_{u(t)} \int_0^{t_f} \Big[\, \lambda\, |u(t)| - \eta(\beta(u(t))) \,\Big]\, \mathrm{d}t \qquad \text{subject to:} \qquad \begin{cases} \ddot{\beta}(t) = u(t) & \beta(t_f) = \beta(0) + 2k\pi \\ \dot{\beta}(t_f) = \dot{\beta}(0) & |u(t)| \leqslant u_{\max} \\ |\beta(t)| < \beta_{\max} & |\phi(t)| < \phi_{\max} \end{cases}$$

*PV cell and antenna requirements may impose additional restrictions on sun and squint angles. However, as is done in Marshall et al. (2018),[11] we choose to account for any reduced sun and squint angle ranges through the transmitted power function, not the pointing constraints.

where λ determines the relative weighting of power-optimality and fuel-optimality and k is an integer that determines the number of complete rotations of the SSPS during the interval $[0, t_f]$. For example, based on the solutions to the power-optimal guidance problem from Marshall et al. (2018)[11] for an SSPS in GEO, $k = 1$ for PV2RF1 and $k = 0$ for PV1RF1. The term $|u(t)|$ minimizes propellant consumption because we assume attitude control is achieved with individual thrusters rigidly mounted to the spacecraft's body axes.[18] Likewise, the term $-\eta(\beta(u(t)))$ maximizes power transmission. When $\lambda = 0$, the solution is power-optimal, i.e., power is maximized independent of thrust or propellant consumption considerations. Similarly, when $\lambda = \infty$, the solution is fuel-optimal, i.e., propellant consumption is minimized independent of any power considerations.

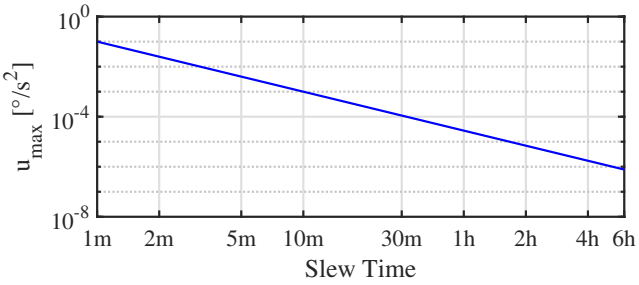

Figure 5: **Angular Acceleration Required for a 90°, Rest-to-Rest Slew Maneuver**

The power-optimal guidance solutions for a dual-sided SSPS include large impulsive slew maneuvers. With the given PV and RF efficiency functions, the instantaneous angle change during these maneuvers is approximately 90°.[11] Because an impulsive slew requires an infinite angular acceleration, this is a singular optimal control problem. To remove these singularities, we impose a finite control constraint, $u_{\max}$. We determine $u_{\max}$ by considering a 90°, bang-bang, rest-to-rest slew maneuver with constant maximum angular acceleration. Figure 5 depicts the relationship between $u_{\max}$ and the slew time for these maneuvers. In this paper, we base the control input constraint on a 10 minute slew. This corresponds to $u_{\max} = 10^{-3}$ °/s^2.

We can easily modify *Problem 2* to account for additional considerations or attitude control system architectures. For example, we can impose angular velocity constraints or formulate the attitude dynamics to include flexibility effects. Alternatively, we can study a momentum-based attitude control system by minimizing the square of the control input and adding constraints on both angular jerk[19] and angular momentum.

Due to its objective function, *Problem 2* is a nonlinear, non-convex optimization problem with linear equality and inequality constraints. Rather than solving it directly, e.g. using nonlinear programming, we instead use a quadratic approximation of the objective function to formulate the problem as a quadratic program (QP). To convert *Problem 2* into a QP, we first discretize the dynamics and pack both the dynamics and periodicity constraints into matrix equalities. We subsequently discretize and approximate the objective function to rewrite *Problem 2* in a form solvable as a QP.

Discrete Dynamics and Periodicity Constraints

In state-space form, the continuous-time dynamics are

$$\underbrace{\begin{bmatrix} \dot{\beta}(t) \\ \ddot{\beta}(t) \end{bmatrix}}_{\dot{\mathbf{x}}(t)} = \underbrace{\begin{bmatrix} 0 & 1 \\ 0 & 0 \end{bmatrix}}_{\mathbf{A}} \underbrace{\begin{bmatrix} \beta(t) \\ \dot{\beta}(t) \end{bmatrix}}_{\mathbf{x}(t)} + \underbrace{\begin{bmatrix} 0 \\ 1 \end{bmatrix}}_{\mathbf{B}} u(t) \tag{11}$$

where $\mathbf{x}(t)$ is the state vector, $u(t)$ is the angular acceleration imparted by the thrusters, $\mathbf{A}$ is the dynamics matrix, and $\mathbf{B}$ is the control influence matrix. Using a zero-order hold (ZOH) parameterization of the control input, we transform Eq. (11) from continuous-time to discrete-time to obtain

$$\dot{\mathbf{x}}(t) = \mathbf{A}\mathbf{x}(t) + \mathbf{B}u(t) \quad \rightarrow \quad \mathbf{x}_{i+1} = \mathbf{A}_d\mathbf{x}_i + \mathbf{B}_d u_i \tag{12}$$

where $i = 0, 1, \ldots, N-1$ denotes the i-th time step, N is the total number of time steps, and $\Delta t = \frac{t_f}{N-1}$ is the length of each time step. $\mathbf{A}_d$ and $\mathbf{B}_d$ are given by

$$\mathbf{A}_d = e^{\mathbf{A}\Delta t} = \begin{bmatrix} 1 & \Delta t \\ 0 & 1 \end{bmatrix} \tag{13}$$

$$\mathbf{B}_d = \left(\int_0^{\Delta t} e^{\mathbf{A}(\Delta t - \tau)} d\tau \right) \mathbf{B} = \begin{bmatrix} \Delta t^2/2 \\ \Delta t \end{bmatrix} \tag{14}$$

However, for linear time-invariant dynamics, the state at time step i is simply a linear combination of the initial state $\mathbf{x}_0$ and the control inputs applied at each previous time step, i.e.,

$$\begin{aligned}
\mathbf{x}_1 &= \mathbf{A}_d \mathbf{x}_0 + \mathbf{B}_d u_0 \\
\mathbf{x}_2 &= \mathbf{A}_d \mathbf{x}_1 + \mathbf{B}_d u_1 = \mathbf{A}_d^2 \mathbf{x}_0 + \mathbf{A}_d \mathbf{B}_d u_0 + \mathbf{B}_d u_1 \\
&\vdots \\
\mathbf{x}_{N-1} &= \mathbf{A}_d^{N-1} \mathbf{x}_0 + \mathbf{A}_d^{N-2} \mathbf{B}_d u_0 + \mathbf{A}_d^{N-3} \mathbf{B}_d u_1 + \ldots + \mathbf{B}_d u_{N-2}
\end{aligned}$$

We can compactly express each of these equations in matrix form, as follows:

$$\mathbf{x}_i = \mathbf{A}_d^i \mathbf{x}_0 + \underbrace{\begin{bmatrix} \mathbf{A}_d^{i-1}\mathbf{B}_d & \mathbf{A}_d^{i-2}\mathbf{B}_d & \ldots & \mathbf{A}_d\mathbf{B}_d & \mathbf{B}_d & \mathbf{0}_{2\times 1} & \ldots & \mathbf{0}_{2\times 1} \end{bmatrix}}_{\mathbf{G}_i} \mathbf{U} \tag{15}$$

where $\mathbf{0}_{2\times 1}$ denotes the 2×1 null vector and $\mathbf{U} = \begin{bmatrix} u_0 & u_1 & \ldots & u_{N-2} \end{bmatrix}^T$. Equivalently,

$$\mathbf{x}_i = \underbrace{\begin{bmatrix} \mathbf{G}_i & \mathbf{A}_d^i \end{bmatrix}}_{\tilde{\mathbf{G}}_i} \underbrace{\begin{bmatrix} \mathbf{U} \\ \mathbf{x}_0 \end{bmatrix}}_{\tilde{\mathbf{U}}} \tag{16}$$

Eq. (15) is convenient for incorporating periodic boundary conditions into the optimal control problem, i.e., we can express the discretized periodic boundary conditions $\beta_{N-1} = \beta_0 + 2k\pi$, $\dot{\beta}_{N-1} = \dot{\beta}_0$ as

$$\underbrace{\begin{bmatrix} \mathbf{G}_{N-1} & \left(\mathbf{A}_d^{N-1} - \mathbf{I}_2\right) \end{bmatrix}}_{\mathbf{C}} \tilde{\mathbf{U}} = \underbrace{\begin{bmatrix} 2k\pi \\ 0 \end{bmatrix}}_{\mathbf{d}} \tag{17}$$

Likewise, Eq. (16) is useful for compactly representing the orientation of the SSPS at time step i, i.e., $\beta_i = \tilde{\mathbf{G}}_i(1,:)\tilde{\mathbf{U}}$ where the notation $\tilde{\mathbf{G}}_i(1,:)$ denotes the first row and all of the columns of $\tilde{\mathbf{G}}_i$. As a result, we can represent the attitude at all N time steps in matrix form by

$$\underbrace{\begin{bmatrix} \beta_0 \\ \beta_1 \\ \vdots \\ \beta_{N-1} \end{bmatrix}}_{\mathbf{f}} = \underbrace{\begin{bmatrix} \tilde{\mathbf{G}}_0(1,:) \\ \tilde{\mathbf{G}}_1(1,:) \\ \vdots \\ \tilde{\mathbf{G}}_{N-1}(1,:) \end{bmatrix}}_{\mathbf{E}} \tilde{\mathbf{U}} \tag{18}$$

Discretization and Approximation of *Problem 2*

Discretizing the objective function from *Problem 2* under a ZOH parameterization of the control input yields

$$\int_0^{t_f} \left[\lambda \left| u(t) \right| - \eta(\beta(u(t))) \right] \, \mathrm{d}t \approx \left(\lambda \sum_{i=0}^{N-2} |u_i| - \sum_{i=0}^{N-1} \eta(\beta_i) \right) \Delta t \tag{19}$$

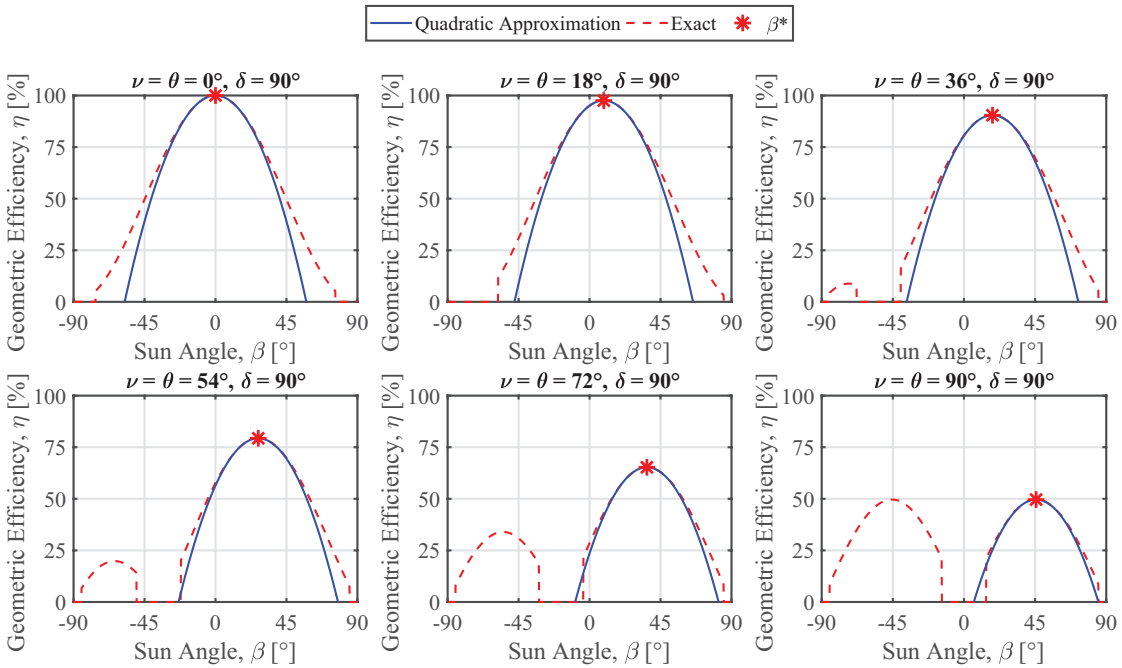

Figure 6: **Quadratic Approximation of the Geometric Efficiency at Various Points in GEO**

We use a quadratic approximation of the geometric efficiency, i.e.,

$$\eta(\beta_i) \approx \eta(\beta_i^*) + \eta'(\beta_i^*)\,(\beta_i - \beta_i^*) + \frac{1}{2}\eta''(\beta_i^*)\,(\beta_i - \beta_i^*)^2 \tag{20}$$

where $\beta_i^* = \beta^*(t_i)$ is a solution to the power-optimal guidance problem (*Problem 1*) and $(\cdot)' = d/d\beta$. Assuming $\eta(\beta)$ is smooth and continuous in the vicinity of β_i^*, then because β_i^* is a maximizer of $\eta(\beta)$, $\eta'(\beta_i^*) = 0$ and $\eta''(\beta_i^*) \leqslant 0$. Thus, we can write Eq. (20) as

$$\eta(\beta_i) \approx \eta(\beta_i^*) - \frac{1}{2}|\eta''(\beta_i^*)|\,(\beta_i - \beta_i^*)^2 \tag{21}$$

where $\eta''(\beta_i^*) \leqslant 0$ implies $\eta''(\beta_i^*) = -|\eta''(\beta_i^*)|$. Figure 6 compares the quadratic approximation of the geometric efficiency, Eq. (21), with the exact geometric efficiency, Eq. (6), at various points in GEO. We only plot the geometric efficiency function for $\nu \in [0°, 90°]$ because the geometric efficiency in GEO ($\delta = 90°$) is antisymmetric about the sun vector ($\theta = 0°$) and the approximation depends on the SSPS architecture (PV2RF2 versus PV1RF1) for $\nu \in (90°, 180°]$. For $\beta_i \in \beta_i^* \pm 10°$, the relative errors between the approximate and exact geometric efficiencies never exceed 0.2% for PV2RF1 and 2% for PV1RF1. Because the errors with the quadratic approximation increase as $|\beta_i - \beta_i^*|$ increases, we only consider optimal attitude maneuvers that are close to $\beta^*(t)$.

Using Eq. (21), the objective functions becomes

$$\int_0^{t_f} \Big[\, \lambda\,|u(t)| - \eta(\beta(u(t)))\,\Big]\,\mathrm{d}t \approx \left(\lambda \sum_{i=0}^{N-2}|u_i| + \frac{1}{2}\sum_{i=0}^{N-1}|\eta''(\beta_i^*)|\,(\beta_i - \beta_i^*)^2 - \sum_{i=0}^{N-1}\eta(\beta_i^*)\right)\Delta t \tag{22}$$

By defining

$$\mathbf{W} = \frac{1}{2}\,\mathrm{diag}\left\{\,|\eta''(\beta_0^*)|, |\eta''(\beta_1^*)|, \ldots, |\eta''(\beta_{N-1}^*)|\,\right\}, \tag{23}$$

using Eq. (18), and noting that both $\sum_{i=0}^{N-1}\eta(\beta_i^*)$ and Δt in Eq. (22) are constants, we arrive at the following discrete, approximate form of *Problem 2*:

Problem 3:

$$\min_{\tilde{\mathbf{U}}} \left\{ \lambda \, ||\mathbf{U}||_1 + \left|\left| \mathbf{W}^{1/2} \left(\mathbf{E}\tilde{\mathbf{U}} - \mathbf{f}^* \right) \right|\right|_2^2 \right\} \quad \text{subject to:} \quad \begin{cases} \mathbf{C}\tilde{\mathbf{U}} = \mathbf{d} \\ |u_i| \leqslant u_{\max}, \quad i = 0, \ldots, N-2 \\ |\beta_i| < \beta_{\max}, \quad i = 0, \ldots, N-2 \\ |\phi_i| < \phi_{\max}, \quad i = 0, \ldots, N-2 \end{cases}$$

where $[\mathbf{f}^*]_i = \beta_i^*$ and the notation $||\cdot||_p$ denotes the l_p-norm of a vector. This is a regularized least squares problem with linear equality and inequality constraints that is readily solvable as a QP.

Intuitively, the l_2-norm in *Problem 3* minimizes the Euclidean distance (subject to various weights) between the attitude trajectories corresponding to $\tilde{\mathbf{U}}$ and $\beta^*(t)$. Hence, in practice, we can ignore the pointing constraints on β and ϕ in *Problem 3* so long as we verify that they are satisfied a posteriori. While this approach works for the GEO and MEO examples in this paper, it is not guaranteed to work in general.

For implementation in CVX,[20,21] we replace the quadratic form in *Problem 3*, i.e., the squared l_2-norm, with an unsquared l_2-norm because quadratic forms are known to cause numerical difficulties in CVX's underlying solvers.[22] With these modifications, we arrive at the following equivalent optimization problem:

Problem 4:

$$\min_{\tilde{\mathbf{U}}} \left\{ \mu \, ||\mathbf{U}||_1 + \left|\left| \mathbf{W}^{1/2} \left(\mathbf{E}\tilde{\mathbf{U}} - \mathbf{f}^* \right) \right|\right|_2 \right\} \quad \text{subject to:} \quad \begin{cases} \mathbf{C}\tilde{\mathbf{U}} = \mathbf{d} \\ |u_i| \leqslant u_{\max}, \quad i = 0, \ldots, N-2 \end{cases}$$

where $\mu \neq \lambda$ is also a relative weighting between power-optimality and fuel-optimality. While *Problem 3* and *Problem 4* are equivalent in the sense that they both trace out the same optimal tradeoff curves, they do not in general produce the same solutions for $\tilde{\mathbf{U}}$ when $\lambda = \mu$. Solutions to *Problem 4* are power-optimal if $\mu = 0$ and fuel-optimal if $\mu = \infty$.

Since we are interested in the tradeoff between power-optimality and fuel-optimality, we are not concerned with the exact values of either λ or μ. Instead, we solve *Problem 4* using CVX and the SDPT3[23,24] solver and sweep over a range of values for $\mu \in [0, \infty)$ to generate the results in this paper. For each μ, we substitute the corresponding $\mathbf{E}\tilde{\mathbf{U}}^*$ into Eq. (6) to compute the optimum geometric efficiencies. Note that because the orbit and attitude dynamics evolve on very different time scales, we normalize the attitude dynamics by the orbit period before solving *Problem 4*. Subsequent values of μ reference this normalized problem.

However, in practice, *Problem 4* is ill-conditioned for small values of μ. In particular, if we define the condition number[25] for some matrix $\mathbf{M}$ as

$$\kappa(\mathbf{M}) \equiv \frac{\sigma_{\max}(\mathbf{M})}{\sigma_{\min}(\mathbf{M})} \tag{24}$$

where $\sigma_{\max}$ and $\sigma_{\min}$ denote the maximum and minimum singular values of $\mathbf{M}$, respectively, we find that $\kappa\left(\mathbf{W}^{1/2}\mathbf{E}\right) \sim 10^{12}$ or greater. Hence, we only obtain sensible solutions without significant numerical instabilities with a non-negligible l_1-norm regularization term. Moreover, because $\mathbf{E}^T\mathbf{W}\mathbf{E}$ is not full rank, and thus, not positive definite, we have no guarantee of finding a unique global minimizer of *Problem 4*.

SIMULATION RESULTS

In this section, we present simulation results for a 25 m × 25 m SSPS in GEO and a 20,184 km circular MEO over the course of a sidereal day (t_f = 86,164 s). The corresponding orbit periods are $T_{\text{GEO}} = t_f$ and $T_{\text{MEO}} = t_f/2$. Our simulations use N = 3,315 time steps which gives $\Delta t = 26$ s.

Moreover, we assume the SSPS has a uniform areal density (ρ) of 1 kg/m^2, a total (dry) mass $M = \rho l^2$, a mass moment of inertia $J = Ml^2/12 = \rho l^4/12$, and electric thrusters with a specific impulse (I_{sp}) of 3000 s. We neglect the mass associated with the thrusters and propellant. Miniaturized electric thrusters with specific impulses on the order of 3,000 s that could be incorporated into a future SSPS are currently under development.[26,27]

With these mass properties, each thruster must provide approximately 23 mN of thrust to achieve the maximum angular acceleration of $u_{\max} = 10^{-3}$ °/s^2 used throughout this paper. This is comparable to the maximum thrust provided by existing Hall effect thrusters for small spacecraft. For example, less than 1 g micro-Hall effect thrusters capable of providing on the order of 10 mN of thrust with specific impulses in excess of 1,000 s have already been demonstrated.[26,27] Multiple co-located tip-mounted thrusters provide a scalable solution for achieving the higher thrust levels required for a larger SSPS.

We begin by introducing several useful scaling relationships that allow the results presented herein to be extended to other SSPS concepts. We subsequently present results for PV2RF1 and PV1RF1 concepts in GEO and MEO. Note that with the given PV and RF efficiency functions, solutions for a PV2RF2 SSPS are identical to the PV2RF1 solutions in GEO and the 20,184 km MEO.[11]

Space Solar Power Satellite Scaling Relationships

The mass flow rate of propellant per thruster is

$$\dot{m}(t) = \frac{1}{I_{sp} g_0} \left[\frac{\rho l^3}{12} |u(t)| \right] \tag{25}$$

where $g_0 = 9.81$ m/s^2 is Earth's standard gravitational acceleration and the bracketed term is the magnitude of the thrust provided by each thruster. Hence, the total mass of propellant consumed from $[0, t_f]$ is

$$M_p = 2 \int_0^{t_f} \dot{m}(t) \, \mathrm{d}t \approx \frac{\rho l^3}{6 I_{sp} g_0} \left(||\mathbf{U}||_1 \Delta t \right) \tag{26}$$

The average transmitted power is

$$\bar{P}_t = \left[\, W_{\mathrm{SF}} \eta_{\mathrm{PV}} \eta_{\mathrm{DC\text{-}RF}} \bar{\eta} \, \right] l^2 \tag{27}$$

where the bracketed term is the average transmitted power density[11] and $\bar{\eta}$ is the average geometric efficiency defined by

$$\bar{\eta} = \frac{1}{t_f} \int_0^{t_f} \eta(t) \, \mathrm{d}t \approx \frac{1}{N} \sum_{i=0}^{N-1} \eta(\beta_i) \tag{28}$$

We use the average geometric efficiency as a non-dimensional analogue for transmitted power.

We can use Eqs. (26)-(28) to scale the results in this paper for other SSPS concepts.

Geostationary Earth Orbit (GEO)

We first present the Pareto optimal curve for the tradeoff between propellant mass and orbit-averaged geometric efficiency for a PV2RF1 SSPS in GEO (Figure 7). We obtain the Pareto curve by solving *Problem 4* for a range of values for the weight between power-optimality and fuel-optimality, μ. The first and last points correspond to $\mu = 10^{-9}$ (the approximate power-optimal solution) and $\mu = \infty$ (the fuel-optimal solution), respectively. Due to the aforementioned ill-conditioning of *Problem 4*, we only obtain realistic solutions for $\mu \geqslant 10^{-9}$. The vertical asymptote is the theoretical maximum orbit-averaged geometric efficiency from the power-optimal guidance problem (*Problem 1*).

Figure 7 highlights the expected result, namely that increasing the orbit-averaged geometric efficiency requires increasingly aggressive slew maneuvers, and hence, more propellant. The fuel-optimal solution ($\mu = \infty$) corresponds to a constant angular velocity slew with no control input. It achieves approximately 75% of the maximum orbit-averaged geometric efficiency with no propellant consumption. Slowly increasing the aggressiveness of the slew maneuvers greatly increases the orbit-averaged geometric efficiency. However, for $\mu < 10^{-6}$, increasing the aggressiveness of the slew maneuvers (decreasing μ) results in diminishing returns, i.e., exhausting more propellant negligibly increases the orbit-averaged geometric efficiency. For example, with $\mu = 10^{-6}$, the system achieves an 81.4% efficiency with only 2.4 kg of propellant, whereas

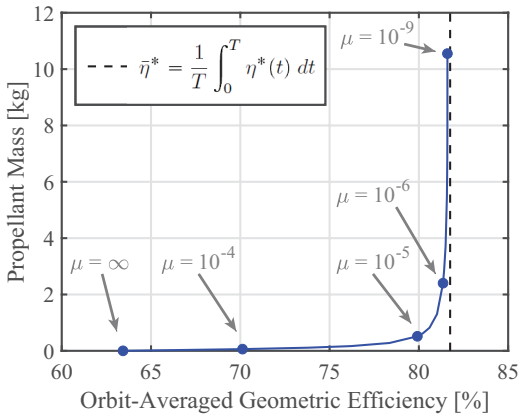

Figure 7: **Pareto optimal curve depicting the tradeoff between propellant mass for an 11 year mission and orbit-averaged geometric efficiency for a dual-sided PV, single-sided RF SSPS in GEO. A few points are marked with the corresponding values of μ.**

with $\mu = 10^{-9}$, it requires 10.6 kg of propellant to achieve a marginally higher efficiency of 81.6%. In both cases, the propellant mass is small relative to the spacecraft's total mass, e.g., for $\mu = 10^{-9}$, the propellant mass for the 11 year mission is 1.7% of the spacecraft's total mass.

To gain intuition into the Pareto optimal curve, we next consider the optimal orientations and geometric efficiencies for various values of μ, as depicted in Figure 8. As previously mentioned, when $\mu = \infty$, we minimize propellant consumption independent of power considerations and obtain a constant angular velocity slew maneuver with no control input. This corresponds with the straight line in Figure 8a. As μ decreases and we begin to weight both power and propellant consumption, we begin to recover increasingly sharp slew maneuvers in the vicinity of $t/T = 0.25$ ($\nu = 90°$) and $t/T = 0.75$ ($\nu = 270°$). Obviously, as the "sharpness" of these maneuvers increases, the maneuver duration decreases. This decrease in maneuver duration corresponds with an increase in the geometric efficiencies immediately before and after the maneuver, as seen in Figure 8b.

Physically, the large slew maneuvers in Figure 8a are optimal because they decrease the sun and squint angles on the active PV and RF surfaces, thereby increasing the system's overall efficiency. In that sense, the maneuvers "switch" the active PV or RF surfaces. For PV2RF1, these maneuvers correspond with switches from the PV 1 to the PV 2 surfaces depicted in Figure 1 and vice versa.

To further reinforce these points, we consider the angular velocities and angular accelerations/control inputs corresponding to the optimal orientations from Figure 8a. These angular velocities and accelerations are plotted in Figures 9a and 9b, respectively. In particular, we see the expected behavior, namely that as μ decreases, both the angular velocity and acceleration substantially increase until the control input saturates at $\pm u_{\max}$. In the absence of this control input constraint, these maneuvers correspond to a singularity whereby the maximum angular velocity and acceleration continually increase as μ decreases. Additionally, Figure 9b depicts the bang-off-bang structure characteristic of fuel-optimal trajectories, i.e., solutions to l_1-norm minimization problems.[18] Specifically, the control input trajectory is punctuated by short duration, high amplitude pulses for attitude corrections. Taken together, these phenomena explain the trends depicted in the Pareto curve of Figure 7. Moreover, these trends agree with the results presented in Figure 7 of Goel et al. (2017)[17] for the attitude trajectories of a formation of PV1RF2 SSPSs in GEO.

Finally, we can compare the PV2RF1 solutions with the PV1RF1 solutions by examining the optimal orientations and geometric efficiencies for several representative values of μ, as depicted in Figures 10a and 10b, respectively. We immediately see from Figure 10a that the PV1RF1 solutions do not feature the large slew maneuvers characteristic of the PV2RF1 solutions. These slew maneuvers are inadmissible with the PV1RF1 pointing constraints. Instead, the solutions for finite μ are characterized by regions with slowly

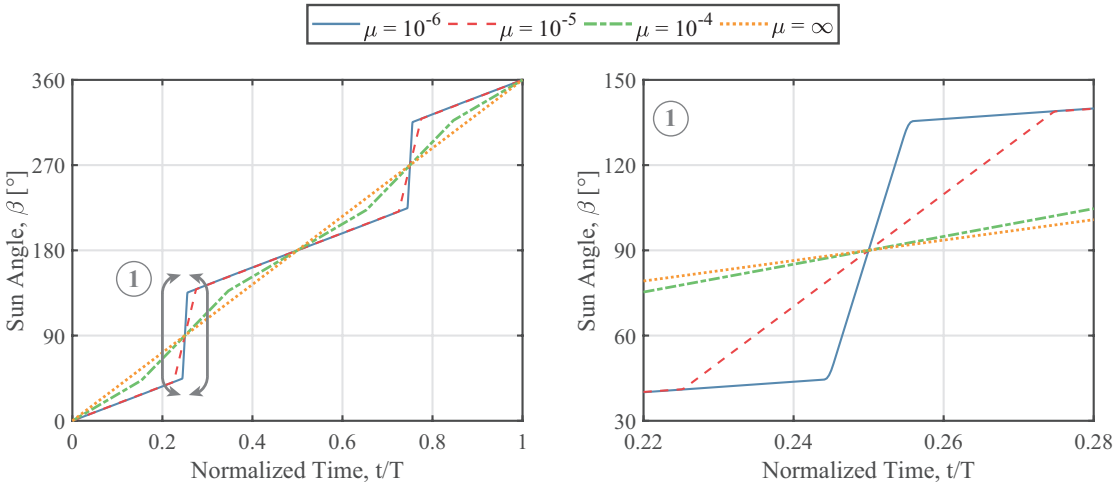

(a) Optimal Orientations

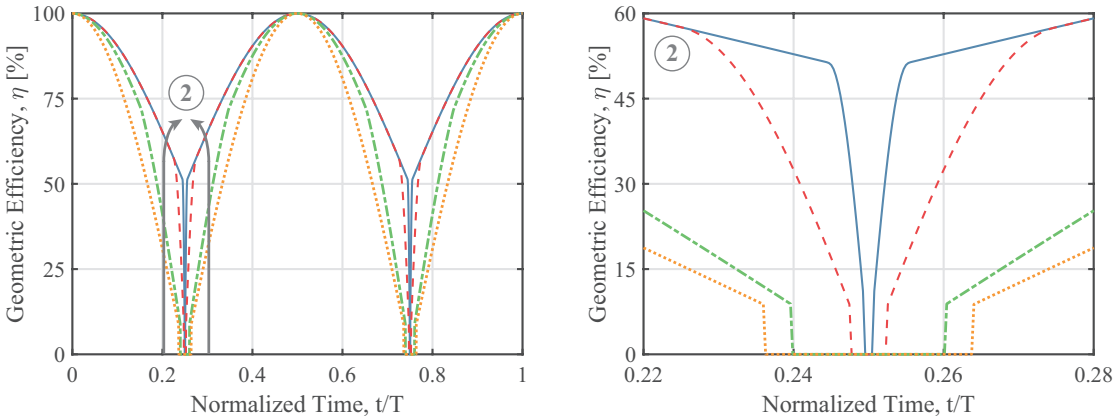

(b) Optimal Geometric Efficiencies

Figure 8: **Solutions to *Problem 4* for a Dual-Sided PV, Single-Sided RF SSPS in GEO**

varying sun angles punctuated by a slow reorientation maneuver. This reorientation maneuver coincides with a dead zone in the vicinity of $\nu = \theta = 180^\circ$ where the SSPS can only orient either its PV surface towards the Sun or its RF surface towards the receiving station, not both. As a consequence, the geometric efficiencies from Figure 10b are zero over a significant portion of the orbit. This explains why PV1RF1 has a significantly lower orbit-averaged geometric efficiency than PV2RF1. The orbit-averaged geometric efficiencies and propellant masses corresponding to the curves in Figure 10 are listed in Table 2. Lastly, note that the special case of $\mu = \infty$ corresponds with a strictly sun-pointing SSPS. In the absence of external disturbances, this sun-pointing solution does not require any control inputs.

In the end, the PV1RF1 attitude dynamics are primarily driven by the orbit geometry that defines the dead zone, as opposed to the singularity that defines the PV2RF1 dynamics. As a result, the PV1RF1 dynamics evolve on longer time scales and require smaller control inputs than the PV2RF1 dynamics. For example, with $\mu = 10^{-6}$, the maximum control inputs for PV2RF1 and PV1RF1 are comparable: 10^{-3} °/s^2 versus 0.8×10^{-3} °/s^2. However, the maximum angular velocities are approximately 0.10 °/s for PV2RF1 and 0.02 °/s for PV1RF1. While the maximum control inputs are comparable because the PV1RF1 solutions also exhibit bang-off-bang behavior, the PV1RF1 SSPS only needs to accelerate for very short durations to achieve the angular velocity necessary to complete the slow reorientation maneuver. This leads to a lower maximum

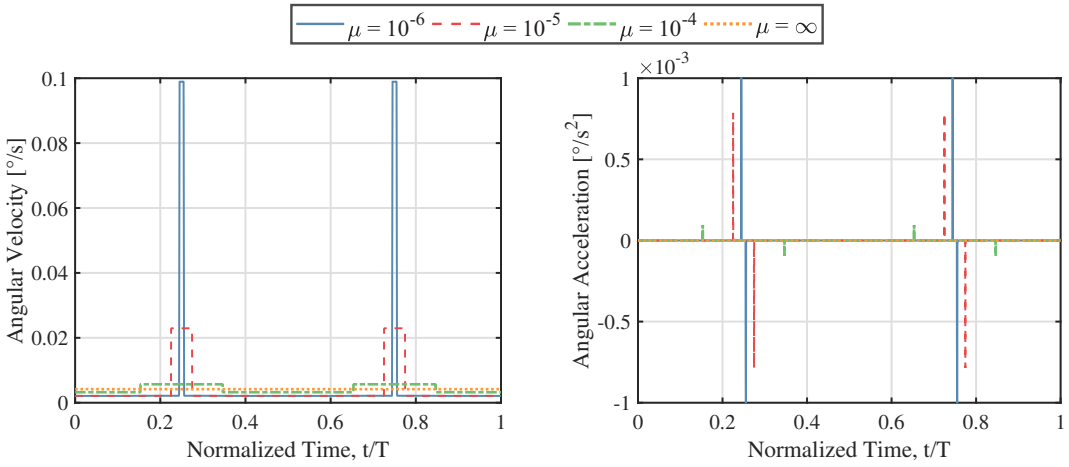

(a) Angular Velocity

(b) Angular Acceleration/Control Input

Figure 9: **Angular Velocities and Accelerations for a Dual-Sided PV, Single-Sided RF SSPS in GEO**

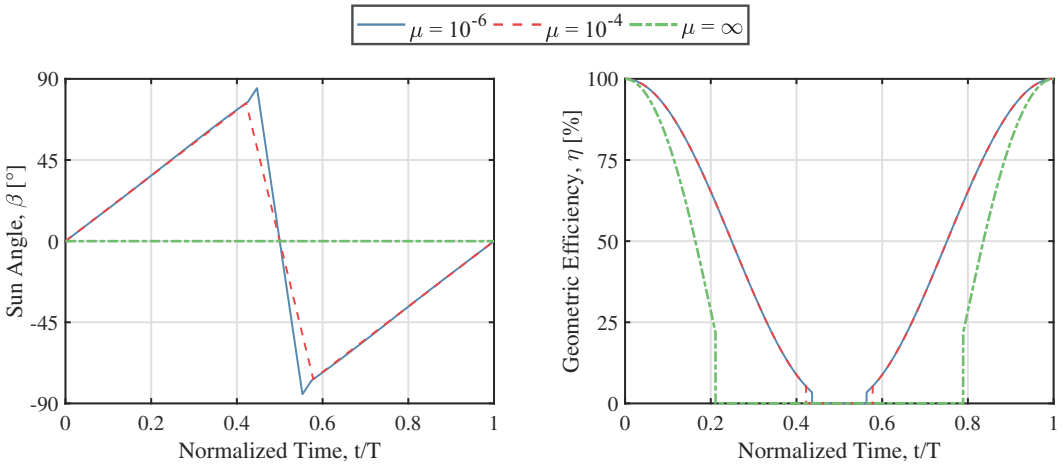

(a) Optimal Orientations

(b) Optimal Geometric Efficiencies

Figure 10: **Solutions to *Problem 4* for a Single-Sided PV, Single-Sided RF SSPS in GEO**

angular velocity for PV1RF1 compared to PV2RF1. Thus, dynamics are a much smaller consideration for PV1RF1 than PV2RF1.

Medium Earth Orbit (MEO)

Figure 11 depicts the Pareto optimal curve for the tradeoff between propellant mass and day-averaged geometric efficiency for a PV2RF1 SSPS in a 20,184 km MEO. Again, because *Problem 4* is ill-conditioned, we only obtain realistic solutions for $\mu \geqslant 10^{-9}$. The vertical asymptote represents the theoretical maximum day-averaged geometric efficiency from the power-optimal guidance problem (*Problem 1*). While qualitatively similar, the day-averaged efficiency in MEO decreases by over 50% compared to the efficiency in GEO without substantially changing the required propellant mass.

Interestingly, the minimum efficiency occurs at $\mu \sim 10^{-3}$, not the expected limiting case of $\mu = \infty$. With $\mu \sim 10^{-3}$, the l_1- and l_2-norms in *Problem 4* are of the same order of magnitude, meaning $\mu \sim 10^{-3}$ corresponds to the transition between solutions that weight power-optimality more than fuel-optimality and

Table 2: **Orbit-averaged geometric efficiencies and propellant masses for representative single-sided PV, single-sided RF solutions in GEO. Propellant masses are for an 11 year mission.**

μ	$\bar{\eta}$ [%]	M_p [kg]
10^{-6}	49.6	0.31
10^{-4}	49.4	0.17
∞	30.6	0

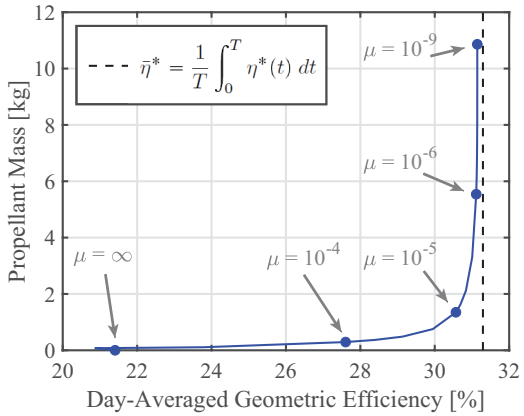

Figure 11: **Pareto optimal curve depicting the tradeoff between propellant mass for an 11 year mission and day-averaged geometric efficiency for a dual-sided PV, single-sided RF SSPS in MEO. A few points are marked with the corresponding values of μ.**

vice versa. Ultimately, while the $\mu = \infty$ case is an exact (albeit numerical) solution, we hypothesize that the quadratic approximation of the objective function is a poor assumption in this transition region. Hence, while the point at $\mu = \infty$ is accurate, the behavior elsewhere in the vicinity of $\mu \sim 10^{-3}$ may not be.

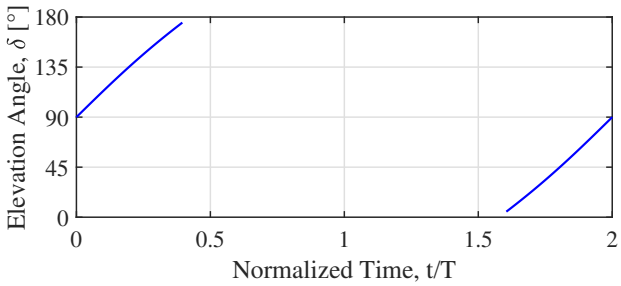

Figure 12: **Elevation Angles for Two Orbits in MEO**

To better understand the efficiency decrease in MEO, we consider the elevation angle profile for two orbits given by Figure 12. When the elevation angles are undefined, the Earth blocks the SSPS's view of the receiving station. Assuming a minimum elevation angle of 5°, then the SSPS transmits to the receiving station for approximately 40% of each day. Hence, we can attribute the decrease in efficiency to the finite time the SSPS has access to the receiving station. While this study is limited in scope to a single spacecraft transmitting to a single receiving station, intermittent access in MEO motivates future studies of SSPS constellations. A constellation of several spacecraft in MEO should be capable of providing persistent coverage to multiple points on Earth, thereby increasing overall system efficiency at the cost of higher total propellant consumption.

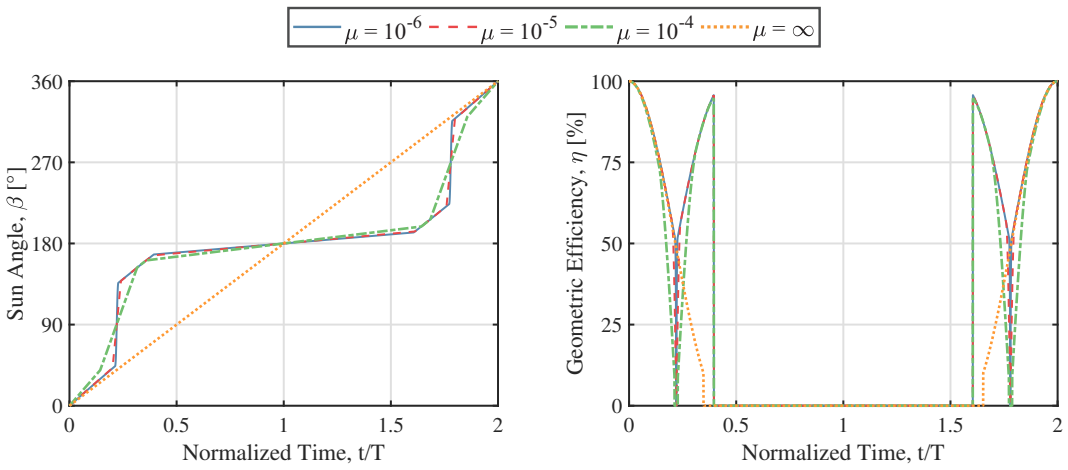

(a) Optimal Orientations

(b) Optimal Geometric Efficiencies

Figure 13: **Solutions to *Problem 4* for a Dual-Sided PV, Single-Sided RF SSPS in MEO**

Figure 13 then plots the optimal orientations and geometric efficiencies for MEO for various values of μ. There are two important observations from Figure 13. First, Figure 13b indicates that the geometric efficiency is zero when the Earth blocks the SSPS's view of the receiving station, as expected. Figure 13a then shows that the SSPS uses the time between receiving station passes to reorient itself for the next pass. Second, because the optimal orientations in MEO feature comparable slew maneuvers to GEO, MEO and GEO have similar propellant requirements.

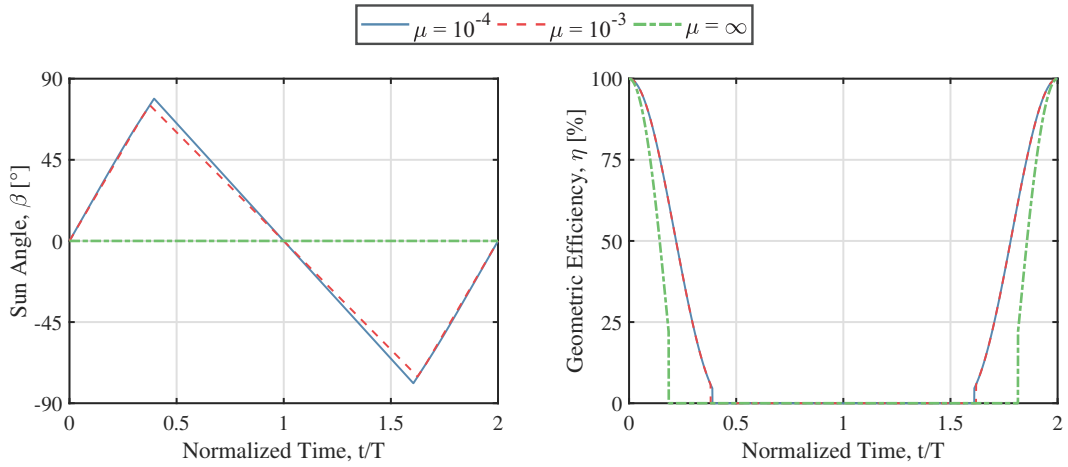

(a) Optimal Orientations

(b) Optimal Geometric Efficiencies

Figure 14: **Solutions to *Problem 4* for a Single-Sided PV, Single-Sided RF SSPS in MEO**

As final points of comparison, we again consider the optimal PV1RF1 orientations and geometric efficiencies for several representative values of μ, as depicted in Figures 14a and 14b, respectively. Like in GEO, these solutions are characterized by slowly varying sun angles and the absence of large slew maneuvers. The only real difference in MEO is that the slow reorientation maneuver now occurs in the large gap between receiving station passes. As a result, both the day-averaged geometric efficiencies and propellant masses for PV1RF1 are lower in MEO than in GEO. The day-averaged geometric efficiencies and propellant masses for the PV1RF1 solutions in Figure 14 are listed in Table 3.

Table 3: **Orbit-averaged geometric efficiencies and propellant masses for representative single-sided PV, single-sided RF solutions in MEO. Propellant masses are for an 11 year mission.**

μ	$\bar{\eta}$ [%]	M_p [kg]
10^{-4}	22.0	0.10
10^{-3}	22.0	0.09
∞	13.4	0

DISCUSSION AND FUTURE WORK

We can use the Pareto curves in Figures 7 and 11 to design the attitude maneuvers for a PV2RF1 SSPS. Because the Pareto curves are parameterized by μ, we simply need to find the value of μ corresponding to some parameter of interest, e.g. propellant mass or maximum angular velocity, to fully specify the attitude maneuvers.

Not surprisingly, the attitude maneuvers are critical structural design drivers. For one, many environmental loads on the structure, like gravity gradients and radiation pressure (e.g. due to solar pressure, microwave pressure, thermal emission/absorption, or Earth albedo), are functions of attitude. Likewise, the angular velocity and acceleration characterize the inertial loads on the structure. In particular, the centripetal and Euler loads are proportional to $\dot{\beta}^2$ and $u = \ddot{\beta}$, respectively. As a first approximation for the SSPS's flexible dynamics, for example, we can incorporate the attitude maneuvers into a model based on the linear theory of elastodynamics.[28] In other words, we can superpose small elastic displacements on top of the SSPS's large overall rigid body motion and solve the corresponding linear elasticity problem in the SSPS's rotating body reference frame. An important next step is to use the results in this paper to quantify flexibility effects.

While our results show that a PV2RF1 SSPS in GEO achieves over twice the efficiency with less than half of the propellant required by its counterpart in MEO, this represents only one facet of a complicated design space. For example, even though propellant requirements are higher in MEO, this is likely outweighed by the reduced launch costs of delivering a spacecraft to MEO. Similarly, while the radiation environment in MEO is harsher than GEO,[29] MEO does not have the overcrowding issues normally associated with GEO. Likewise, a small constellation of satellites in MEO can achieve persistent coverage over multiple locations on Earth, whereas a spacecraft in GEO only achieves persistent coverage over a single location. The takeaway is that it is naive to specify the orbit for an SSPS based solely on system efficiency and propellant consumption considerations. Regardless, in all cases, the ACS propellant mass is small relative to the total mass of the spacecraft.

Another key design consideration is dual-sided versus single-sided. While the results presented elsewhere[11,16,17] show that dual-sided operations significantly increase overall system efficiency, it is yet to be seen if this performance boost actually outweighs the technical complexity, mass penalty, and cost associated with implementing either RF-transparent PV or optically-transparent RF surfaces. Moreover, this efficiency trade neglects attitude dynamics considerations. Specifically, for an ultralight, planar, dual-sided SSPS, structural excitation due to attitude maneuvers may have a detrimental effect on system performance. Due to the absence of large slew maneuvers, a PV1RF1 architecture may remove these attitude dynamics considerations altogether.

Interestingly, for a PV2RF1 SSPS in both GEO and MEO, the fuel-optimal solutions, i.e., the solutions that minimize propellant consumption independent of power considerations, achieve approximately 70% or more of the maximum possible geometric efficiencies without any control inputs. These constant slew rate maneuvers are potentially advantageous for minimizing excitation of flexible modes. Hence, there may be interesting structural and system level design trades associated with these maneuvers.

In this paper, we have intentionally limited our scope to circular, equatorial orbits and equatorial receiving stations. As a result, a logical extension of this work is to treat eccentric and/or inclined orbits and non-equatorial receiving stations. By doing so, the orbit-attitude coupling relation, Eq. (1), becomes nonlinear,

making the optimization problem significantly more difficult to solve. While we currently specify the orbit and solve for the optimal attitude trajectory, a further extension is to reformulate the attitude maneuver design problem to simultaneously solve for both the optimal orbit and attitude trajectory.

Our analysis also neglects both orbit and attitude disturbances. We can easily accommodate gravitational orbit perturbations like J2 and third-body effects into the existing attitude maneuver design framework. However, non-gravitational perturbations like solar pressure are more challenging. Specifically, because solar pressure depends on attitude, any attempt to model solar pressure effects must account for the coupled orbit and attitude dynamics of the SSPS. Radiation pressure perturbations are proportional to area-to-mass ratio, i.e., the inverse of areal density. At the areal densities of 0.1 kg/m^2 to 1 kg/m^2 envisioned for future ultralight SSPS concepts,[8] solar pressure is likely a significant perturbation over the lifetime of the spacecraft.[30] Ultimately, quantifying the SSPS's disturbance environment is important for estimating attitude disturbance rejection and stationkeeping requirements.

Additionally, it would be useful to more thoroughly study the accuracy of the quadratic approximation scheme. For PV2RF1 in MEO, we have already seen that the quadratic approximation is likely a poor assumption for values of μ that correspond to the transition between solutions that weight power-optimality more than fuel-optimality. Solving the original, nonlinear, non-convex optimization problem (*Problem 2*) with sequential convex programming[17] may provide more accurate solutions for these values of μ. It would also be valuable to compare our results with results obtained from solving *Problem 2* using something like nonlinear programming or a genetic algorithm.

Finally, the attitude maneuver design problem presented in this paper is only one of the numerous guidance, navigation, and control challenges associated with flying an SSPS. For example, future work can explore the ACS actuator and sensor trade spaces or investigate ACS-structure interaction. While this work baselines a rather conventional ACS with tip-mounted thrusters, novel sensor and actuator concepts, like those based on large numbers of distributed sensors and actuators, may prove beneficial for addressing some of the challenges of flying ultralight, flexible spacecraft.

CONCLUSION

This paper formulates and solves the attitude maneuver design problem for a planar SSPS. We first show how we can approximate the original, nonlinear, non-convex optimization problem governing the attitude maneuvers with a quadratic program. Subsequently, we solve the attitude maneuver design problem for SSPSs in both GEO and a 20,184 km MEO to study attitude dynamics and to estimate system efficiencies and propellant masses. The resulting Pareto curves contain all of the information necessary for designing attitude maneuvers for a planar SSPS. These Pareto curves highlight how a point is ultimately reached where increasing control and hence, propellant consumption, negligibly increases overall system efficiency. Moreover, they show that fuel-optimal solutions, i.e. the solution where fuel is minimized independent of any power considerations, achieve approximately 75% of the maximum possible system efficiency without expending any propellant. Ultimately, these results highlight how attitude dynamics are a critical design driver for planar SSPS concepts.

ACKNOWLEDGMENT

We thank the Caltech Space Solar Power Project team, especially Dr. Dan Scharf (NASA-JPL), Dr. Richard Madonna (Caltech), and Dr. Terry Gdoutos (Caltech), for helpful comments and discussions. M.M. was supported by a NASA Space Technology Research Fellowship. Financial support from the Space Solar Power Project at Caltech is also acknowledged.

REFERENCES

[1] I. Asimov, "Reason," *I, Robot*, 1941, pp. 59–77.

[2] P. E. Glaser, "Power from the Sun: Its Future," *Science*, Vol. 162, No. 3856, 1968, pp. 857–861, 10.1126/science.162.3856.857.

[3] C. Carrington, J. Fikes, M. Gerry, D. Perkinson, H. Feingold, and J. Olds, "The Abacus/Reflector and integrated symmetrical concentrator - Concepts for space solar power collection and transmission," *35th Intersociety Energy Conversion Engineering Conference and Exhibit*, International Energy Conversion Engineering Conference (IECEC), Las Vegas, Nevada, 2000, 10.2514/6.2000-3067.

[4] J. C. Mankins, "A Technical Overview of the "SunTower" Solar Power Satellite Concept," *Acta Astronautica*, Vol. 50, 2002, pp. 369–377, 10.1016/S0094-5765(01)00167-9.

[5] S. Sasaki, K. Tanaka, K. Higuchi, N. Okuizumi, S. Kawasaki, N. Shinohara, K. Senda, and K. Ishimura, "A new concept of solar power satellite: Tethered-SPS," *Acta Astronautica*, Vol. 60, 2007, pp. 153–165, 10.1016/j.actaastro.2006.07.010.

[6] Q. Li, Z. Deng, K. Zhang, and B. Wang, "Precise Attitude Control of Multirotary-Joint Solar-Power Satellite," *Journal of Guidance, Control, and Dynamics*, Vol. 41, No. 6, 2018, pp. 1435–1442, 10.2514/1.G003309.

[7] J. C. Mankins, "New directions for space solar power," *Acta Astronautica*, Vol. 65, No. 1–2, 2009, pp. 146–156, 10.1016/j.actaastro.2009.01.032.

[8] M. Arya, N. Lee, and S. Pellegrino, "Ultralight Structures for Space Solar Power Satellites," *3rd AIAA Spacecraft Structures Conference*, AIAA SciTech Forum, San Diego, California, 2016, 10.2514/6.2016-1950.

[9] P. Jaffe and J. McSpadden, "Energy Conversion and Transmission Modules for Space Solar Power," *Proceedings of the IEEE*, Vol. 101, June 2013, pp. 1424–1437, 10.1109/JPROC.2013.2252591.

[10] E. E. Gdoutos, C. Leclerc, F. Royer, M. D. Kelzenberg, E. C. Warmann, P. Espinet-Gonzalez, N. Vaidya, F. Bohn, B. Abiri, M. R. Hashemi, M. Gal-Katziri, A. Fikes, H. Atwater, A. Hajimiri, and S. Pellegrino, "A Lightweight Tile Structure Integrating Photovoltaic Conversion and RF Power Transfer for Space Solar Power Applications," *2018 AIAA Spacecraft Structures Conference*, AIAA SciTech Forum, Kissimmee, Florida, 2018, 10.2514/6.2018-2202.

[11] M. A. Marshall, A. Goel, and S. Pellegrino, "Power-Optimal Guidance for Planar Space Solar Power Satellites," 2019. In preparation.

[12] B. Wie and C. Roithmayr, "Integrated orbit, attitude, and structural control system design for space solar power satellites," *AIAA Guidance, Navigation, and Control Conference and Exhibit*, Guidance, Navigation, and Control and Co-located Conferences, Montreal, Canada, 2001, 10.2514/6.2001-4273.

[13] B. Wie and C. M. Roithmayr, "Attitude and Orbit Control of a Very Large Geostationary Solar Power Satellite," *Journal of Guidance, Control, and Dynamics*, Vol. 28, No. 3, 2005, pp. 439–451, 10.2514/1.6813.

[14] I. J. McNally, D. J. Scheeres, and G. Radice, "Attitude Dynamics of Large Geosynchronous Solar Power Satellites," *AIAA/AAS Astrodynamics Specialist Conference, AIAA SPACE Forum*, San Diego, California, 2014, 10.2514/6.2014-4123.

[15] S. Wu, K. Zhang, H. Peng, Z. Wu, and G. Radice, "Robust optimal sun-pointing control of a large solar power satellite," *Acta Astronautica*, Vol. 127, 2016, pp. 226–234, 10.1016/j.actaastro.2016.05.019.

[16] A. Goel, N. Lee, and S. Pellegrino, "Trajectory design of formation flying constellation for space-based solar power," *2017 IEEE Aerospace Conference*, Big Sky, Montana, 2017, pp. 1–11, 10.1109/AERO.2017.7943711.

[17] A. Goel, S.-J. Chung, and S. Pellegrino, "Trajectory Design of a Spacecraft Formation for Space-Based Solar Power Using Sequential Convex Programming," *Proceedings 9th International Workshop on Satellites Constellations and Formation Flying (IWSCFF)*, Boulder, Colorado, 2017, pp. 1–20.

[18] I. M. Ross, "Space Trajectory Optimization and L^1-Optimal Control Problems," *Modern Astrodynamics* (P. Gurfil, ed.), Vol. 1 of *Elsevier Astrodynamics Series*, ch. 6, pp. 155–188, Oxford: Butterworth-Heinemann, 2006.

[19] F. A. Leve, B. J. Hamilton, and M. A. Peck, *Spacecraft Momentum Control Systems*, ch. 3, pp. 35–56. Switzerland: Springer International Publishing, 2015, 10.1007/978-3-319-22563-0.

[20] M. Grant and S. Boyd, "CVX: Matlab Software for Disciplined Convex Programming, version 2.1," `http://cvxr.com/cvx`, March 2014.

[21] M. Grant and S. Boyd, "Graph implementations for nonsmooth convex programs," *Recent Advances in Learning and Control* (V. Blondel, S. Boyd, and H. Kimura, eds.), Lecture Notes in Control and Information Sciences, pp. 95–110, Springer-Verlag Limited, 2008. `http://stanford.edu/~boyd/graph_dcp.html`.

[22] M. Grant and S. Boyd, "The CVX Users' Guide, Release 2.1," `http://cvxr.com/cvx/doc/CVX.pdf`, December 2017.

[23] K. C. Toh, M. J. Todd, and R. H. Tütüncü, "SDPT3 — A Matlab software package for semidefinite programming, Version 1.3," *Optimization Methods and Software*, Vol. 11, No. 1-4, 1999, pp. 545–581, 10.1080/10556789908805762.

[24] R. H. Tütüncü, K. C. Toh, and M. J. Todd, "Solving semidefinite-quadratic-linear programs using SDPT3," *Mathematical Programming*, Vol. 95, No. 2, 2003, pp. 189–217, 10.1007/s10107-002-0347-5.

[25] S. Boyd and L. Vandenberghe, *Convex Optimization*. Cambridge, England: Cambridge University Press, 2009.

[26] J. Mueller, R. Hofer, and J. Ziemer, "Survey of Propulsion Technologies Applicable to Cubesats," *Joint Army-Navy-NASA-Air Force (JANNAF)*, Colorado Springs, Colorado, 2010, pp. 1–58.

[27] "Small Spacecraft Technology State of the Art," Tech. Rep. NASA/TP–2015–216648/REV1, Ames Research Center, Moffett Field, California, December 2015.

[28] A. A. Shabana, "Flexible Multibody Dynamics: Review of Past and Recent Developments," *Multibody System Dynamics*, Vol. 1, No. 2, 1997, pp. 189–222, 10.1023/A:1009773505418.

[29] W. J. Larson and J. R. Wertz, *Space Mission Analysis and Design*, ch. 8. El Segundo, California and Dordrecht, The Netherlands: Microcosm Press and Kluwer Academic Publishers, 3 ed., 1999.

[30] D. J. Scheeres, A. Rosengren, and J. McMahon, "The Dynamics of High Area-to-Mass Ratio Objects in Earth Orbit: The Effect of Solar Radiation Pressure," *21st AAS/AIAA Spaceflight Mechanics Meeting*, New Orleans, Louisiana, 2011, pp. 1–25.